Int. J. Heat Mass Transfer. Vol. 34, No. 7, pp. 1633–1647, 1991
Printed in Great Britain

0017-9310/91 $3.00+0.00

The influence of large eddies on thermal mixing

M. R. DAVIS
Department of Civil and Mechanical Engineering, University of Tasmania, Hobart, Tasmania 7001, Australia

and

P. RERKSHANANDANA
King Mongkut's Institute of Technology, Thonburi, Thailand

(*Received* 12 *February* 1990 *and in final form* 7 *September* 1990)

Abstract—The influence of upstream excitation level on the mixing of heat and momentum in a circular jet is investigated, and it is found that there is a direct dependence of the coherent heat transport on the strength of this excitation. The coherent structures do not influence the mean velocity distributions near the nozzle, but further downstream break up and then contribute to increased and similar mixing of average heat and momentum in the flow. Optical observations show that the coherent structures are in the form of toroidal vortices having approximately elliptical cross-sections in the torus, and occur at a rate which is broadly consistent with the magnitude of the coherent heat flux in the initial annular region of the flow.

1. INTRODUCTION

EXPERIMENTAL observations of the turbulent diffusion of momentum and heat in turbulent shear flows have generally provided an indication of close similarities between momentum and thermal diffusivities provided that Reynolds numbers are sufficiently large [1–8]. Whilst the presence of intermittency in mixing shear layers has been evident in some observations [4, 9], in the main investigations have provided a basis for the development of numerical solutions of turbulent diffusion in shear flows by various closure methods such as the k–ε method based on turbulence energy and dissipation [10–16].

The response of mixing layers and jets to applied external perturbations, most commonly of acoustic form originating from upstream in the flow and of impulsive or periodic form, has shown an enhanced tendency for more regular structures to occur in the turbulent mixing zone [17–22], in particular in the initial annular mixing layer of circular jets. Whilst the response of the mixing layer is expected to be non-linear on account of the rolling up of individual vortices by pairing mechanisms having a preferred direction of rotation, the influence of excitation level and frequency on the strength of the induced structures is not well understood. However, detailed observations in plane mixing layers [23–25] and in mixing jets [26–28] have confirmed the general vortex-like character of regular disturbances in mixing shear layers and the presence of pairing mechanisms as the layer develops and thickens [29]. It has also been observed that vortex rings themselves become unstable and can develop peripheral variations of structure [30].

Large-scale eddy structures embedded in a turbulent mixing shear layer introduce an augmentation of the rate of transport of heat and other scalar contaminants in a direction perpendicular to the mean flow. As a consequence the similarity between transverse diffusion of momentum and heat becomes modified [31] and a potential for significantly enhanced thermal diffusion arises. The extent to which this actually occurs in a mixing shear layer depends upon the relative strength and frequency of occurrence of the large-scale eddies which gives rise to bulk mixing effects. Whilst the general physical structure of large-scale eddies is relatively well known from the investigations discussed in preceding paragraphs, the magnitude of their contribution to thermal mixing is less certain and is clearly influenced by Reynolds number, excitation and geometric parameters.

Computations of shear layer development including the effects of large-scale mixing motions have been carried out by large eddy simulations with subgrid scale turbulent diffusion [31–34]. The validation of such approaches must ultimately involve reconciliation of computed results with experimentally observed results. It is one of the purposes of the work to be described to consider the consistency of experimentally observed thermal diffusion which is enhanced by large-scale eddies with observation of the eddy structure and their dependence upon excitation of the shear layer emanating from upstream. In view of the limited experimental data available from the present work, which encompasses mixing regions dominated by regular mixing near the nozzle and by random mixing further downstream, a relatively simple computational approach is used here. In this k–ε modelling is used to predict turbulent mixing rates whilst the coherent mixing which influences thermal

diffusion is matched directly to the experimental observations at various distances from the nozzle. It was not considered at this stage that the data available was sufficiently detailed to merit a more complex numerical approach.

Observations of turbulent and large eddy structures were made in the present investigation by means of the quantitative cross beam schlieren method [21, 22, 35, 36]. In the present work this has been developed to make use of its spatial averaging characteristics along the sensing beams so as to yield information relating directly to the large-scale structures in the flow near to the nozzle exit. Further downstream where these structures are no longer evident the quantitative schlieren is used to determine the scales and spectral characteristics of the random mixing which then predominates.

2. OBSERVATION OF TURBULENT MIXING STRUCTURES

2.1. *Nozzle exit conditions*

The experimental work to be described was carried out in the initial or annular mixing layer of the discharge from a smooth circular nozzle 20 mm in diameter (Fig. 1). The flow was directed vertically upwards so as to avoid any distortion of the flow symmetry due to buoyant gravitational effects. The nozzle internal contour formed a smooth contraction with a parallel exit and was designed using a pair of matched cubic profiles in the concave and convex sections which ensure zero curvature of the nozzle surface at the exit plane. The nozzle was mounted on a 60 mm circular plenum chamber containing two flow smoothing gauze screens and honeycomb flow straighteners. During the initial testing of the nozzle care was taken to ensure that the distribution of temperature of the flow across the exit plane was uniform by coating the plenum chamber and contraction surfaces with a 5 mm thickness of insulating foam covered by a smooth metallic foil overlay. Variations of mean temperature were within 3% of the overall difference between discharge and ambient temperatures. The mean temperature profile at the exit plane reduced sharply from the uniform value in the heated flow to near ambient in a distance of less than 10% of the nozzle diameter. It was difficult to measure the gradient of temperature near the nozzle exit accurately, but it would appear that the integral thickness of the boundary layer at the exit plane of the nozzle was approximately 0.5 mm and it was not considered that this could be improved upon.

Hot wire measurements indicated the nozzle exit boundary layer to be laminar and subject only to acoustic disturbances emanating from upstream which influenced the entire exit flow. Acoustic disturbances originated in the supply of air from a compressed air line through an electric flow heater and four supply lines to symmetrically feed the heated air flow to the plenum chamber. Hot wire measurements (Fig. 2) showed these disturbances to occur at a Strouhal number based on nozzle exit diameter and speed of $St = fd/U_j$ between 0.45 and 0.5 which could be varied somewhat depending on the supply pipe geometry. The fluctuating velocity energy spectrum at the nozzle exit generally showed one or two dominant peaks in this rather narrow range the amplitude of which could be reduced by insertion of acoustically absorbing but flow porous plugs in the supply lines. In this manner two conditions of flow excitation at the nozzle exit could be established with fluctuation levels of 3.6 and 1.4% of the mean exit flow velocity and with a Strouhal number of the dominant spectral peak of 0.50. These fluctuations were found by hot wire traverse to

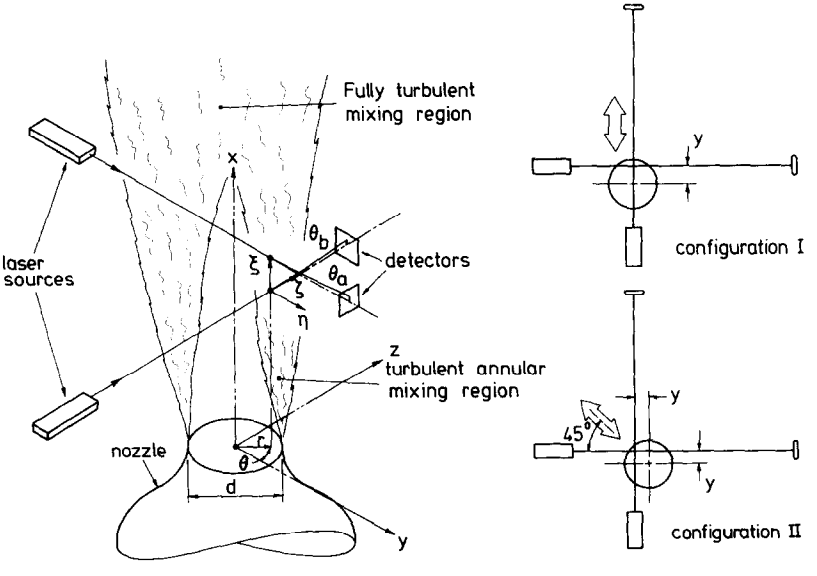

FIG. 1. General arrangement of experimental system.

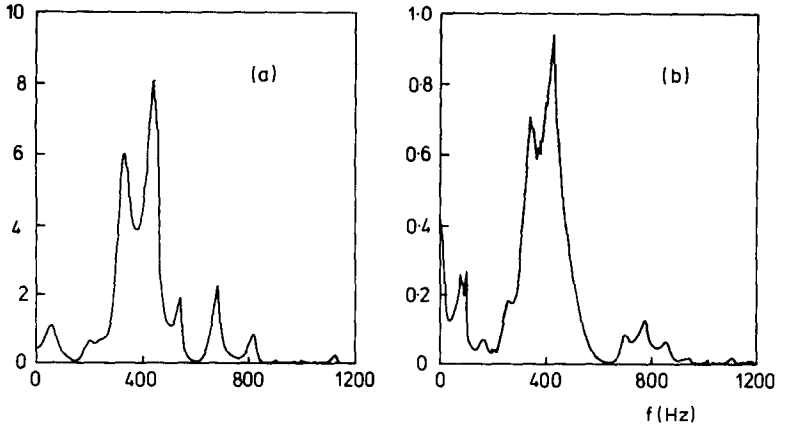

FIG. 2. Spectra of axial component velocity fluctuations at the centre of the nozzle exit plane. (a) $\sqrt{(u'^2)} = 0.036U_j$. (b) $\sqrt{(u'^2)} = 0.014U_j$ ($U_j = 17.1$ m s^{-1}, $T_j - T_a = 0$°C, vertical ordinate: $E_u(f)$ $(10^5/U_j^2)$).

be uniformly distributed over the nozzle exit plane and provided very good conditions for observation of the effect of coherent structures on the mixing process since their amplitude and Strouhal number were well matched to the range of known strong responsiveness of jet mixing to excitation [20–22]. The distribution of turbulent velocity fluctuations along the nozzle axis is shown in Fig. 3, and it can be seen that even though the exit plane turbulence level is below 5%, the turbulence level outside the nozzle is much higher and is sensitive to the excitation level. Only beyond $x/d = 8$ does the influence of exit plane disturbances appear to have been obscured by the shear layer induced turbulent mixing motion.

2.2. *Detection of mixing characteristics by crossed beam axial deflection correlations*

The dynamic, quantitative cross beam schlieren system has been described in detail previously [35, 36] and consisted of two 0.5 mW laser beams mounted perpendicular to each other and to the flow axis. Deflection sensing photodiodes sensed the unsteady deflection of these beams in both coordinate directions due to refractive index gradient fluctuations in the flow. As the flow speed was not high (17 m s^{-1}) the refractive index fluctuations could be directly related to the temperature fluctuations of the heated nozzle air flow as it mixed with ambient air. The nozzle air flow was operated at 40°C above the ambient air temperature (which was in the range 15–22°C).

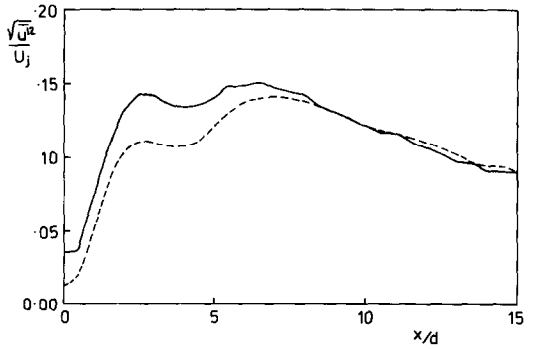

FIG. 3. Distribution of r.m.s. turbulence fluctuations along the flow axis for different exit plane disturbance levels at $St = 0.50$. Solid line, 3.6% velocity fluctuation at nozzle exit. Dashed line, 1.3% velocity fluctuation at nozzle exit.

If a detecting laser beam is traversed over a section of the flow at a fixed distance from the nozzle such that the distance from the beam to the flow axis (Y) varies, then in an isotropic turbulent field it can be shown [35] that the mean square fluctuating beam angular deflection in the axial direction $\overline{\theta_a^2}(Y)$ is given by

$$\overline{\theta_a^2}(Y) = \int_Y^\infty 2f_a(r)\frac{r\,\mathrm{d}r}{\sqrt{(r^2 - Y^2)}} \tag{1}$$

where $f_a(r)$ is the product of the mean square refractive index axial component gradient fluctuation $(\overline{\partial n/\partial x})_r^2$ and the integral scale of these fluctuations in the cross-section plane $l(r)$

$$f_a(r) = \left(\overline{\frac{\partial n}{\partial x}}\right)_r^2 l(r). \tag{2}$$

The integral scale $l(r)$ is defined conventionally as the area under the two-point space correlation diagram of the fluctuations detected. It is thus possible to measure $\overline{\theta_a^2}(Y)$ and apply the Abel integral transformation [37] to determine $f_a(r)$.

Measurement can also be made of the cross correlation coefficient and covariance $(\overline{\theta_a\theta_b})$, between the fluctuating deflections of the two perpendicular detection beams [35] and if the beams intersect at a distance r_i from the flow axis then [38]

$$\overline{\theta_a\theta_b}(r_i) = \left(\overline{\frac{\partial n}{\partial x}}\right)_{r_i}^2 (l(r_i))^2 = 2\pi\overline{(n^2)}_{r_i}. \tag{3}$$

It is thus possible to combine measurements of $\overline{\theta_a^2}(Y)$ and $\overline{\theta_a\theta_b}(r_i)$ and determine $(\overline{\partial n/\partial x})_r^2$ and $l(r)$ separ-

ately. Moreover, it is possible to make such fluctuation measurements either by moving a single beam whilst the other is maintained at a fixed position through the flow axis or by moving both beams to a distance Y from the flow axis (so that $r_1 = \sqrt{2}Y$) referred to as configuration I and configuration II subsequently. Comparison of the results obtained for $l(r)$ by these two configurations has been used [36] to demonstrate negligible directional variation of the integral scale in the cross-sectional plane in the fully turbulent zone of a mixing jet at high Reynolds number, thereby verifying the underlying assumption of isotropy inherent in this method of analysis of observed data to determine fluctuation intensity and integral scale distributions over a cross-section of the flow.

In the present experiments measurements have been made in both the fully turbulent and initial region of the mixing jet flow and the results are shown in Fig. 4(a). In the absence of any large-scale coherent structure effects the cross beam covariance of axial beam deflections is expected to be independent of beam orientation and this is approximately the case at $x/d = 15$ where the results of both configuration I and configuration II observations are similar (Fig. 4(a)(ii)). Close to the nozzle however this is no longer the case (Fig. 4(a)(i)) and it is concluded that there are significant coherent or large-scale motions in the total fluctuations present in the initial annular shear layer. It should be noted that these results are not conditionally sampled in any way and that the cross beam covariance was measured directly by passing the two axial deflection signals generated by the deflection sensing photodiodes (United Detector Technology PIN-SC-10) to an analogue multiplier and averager. Therefore, the results are a reflection of the total fluctuations present in the mixing flow and indicate a substantial coherent structure content near to the nozzle.

Physically the higher level of coherence detected at $x/d = 1.5$ with both beams traversed away from the flow centreline (so as to intersect at 45° to the radius to their intersection point) is a consequence of coherence over the cross-sectional plane perpendicular to the flow. In the configuration II traverse the two-beam covariance is increased by the correlated components of the total signal which originate well away from the intersection point and which are strongest at positions where the beams reach their closest distance from the flow axis. The effect of coherent structures on the two-beam covariance was demonstrated by assuming a series of toroidal vortices with elliptic cross-sections gave rise to the detected cross beam covariance which was then computed. This simulation gave rise to the results of Fig. 4(b), and it can be seen that the form of the covariance distributions closely resembles the observed distribution of Fig. 4(a)(i) in the initial region close to the nozzle. These results thus confirm that the experimental flow contains a substantial component of unsteady mixing eddies of coherent form. Evidence for the assumed elliptical cross-section of the regular vortex structures is discussed subsequently in Section 2.3.

In the fully turbulent region the experimental results of Fig. 4(a)(ii) can be combined with the distribution of mean square axial deflections of either of the traversing schlieren beams to yield the integral scale of the turbulent density gradient fluctuations. This is shown in Fig. 5, and it can be seen that at the centre of the flow ratio of the turbulent integral scale to distance from the nozzle (x) is $l/x = 0.012$. This

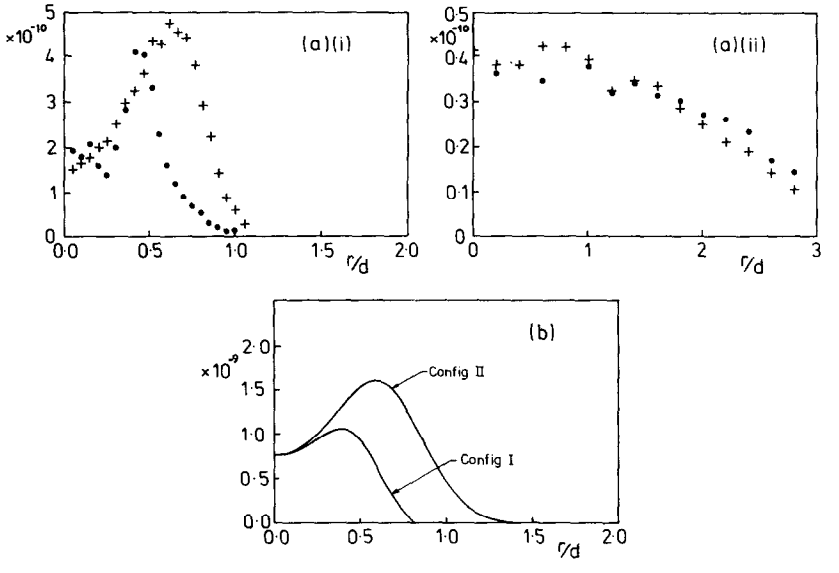

FIG. 4. Distribution of covariance of cross beam schlieren axial component deflections (vertical axis $-\overline{\theta_a\theta_b}$ (rad^2)). (a) Experimentally observed: ●, configuration I; +, configuration II: (i) $x/d = 1.5$; (ii) $x/d = 15$. (b) Computed from elliptic cross-section toroidal vortex model with $b/a = 3$, $L/d = 1.4$, $\rho_m = 0.13$, $\phi = 5\pi/8$.

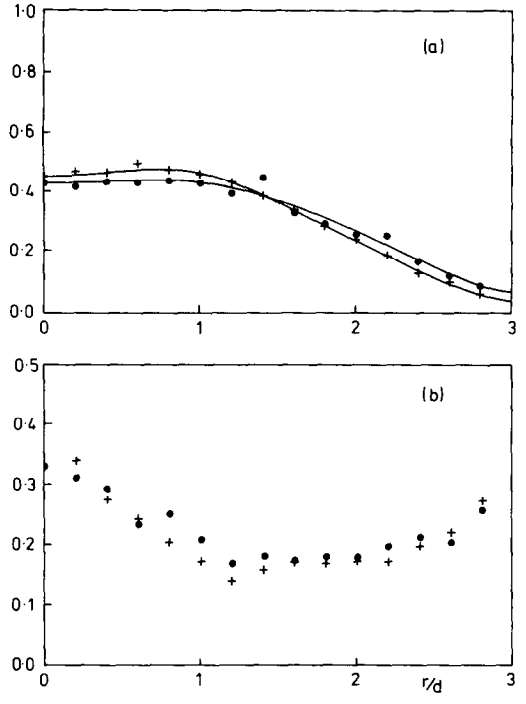

FIG. 5. Distribution of detection beam axial component fluctuations and turbulent integral scale at $x/d = 15$. (a) Mean square beam deflection $\overline{\theta_a^2}(Y)$ (rad$^2 \times 10^9$). (b) Turbulence integral scale $l(r)/d$.

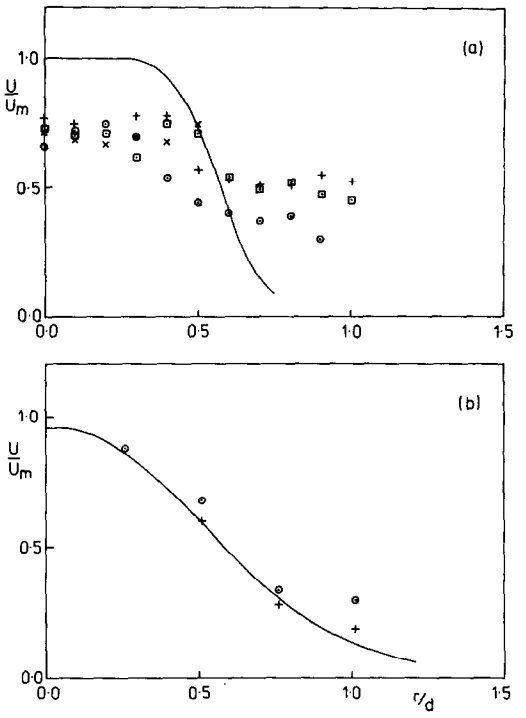

FIG. 6. Distribution of convection velocity detected by the time delay of the maximum covariance of the cross beam system separated in the streamwise direction. (a) $x/d = 1.5$: separation of beams $(\Delta\xi)$: ⊙, 0.5 (configuration I); ⊡, −0.5 (configuration I); +, 0.5 (configuration II); [·], 0.5 (configuration II). (b) $x/d = 15$, $\Delta\xi/d = 0.5$: +, configuration I; ⊙, configuration II. Solid lines, computed velocity. Points, optically observed turbulent convection velocity.

result is in good general accord with previous observations of this ratio [35, 36], and indicates that the coherent structures have broken up into random eddies in the fully turbulent self preserving region as these previous observations were at higher nozzle Reynolds number and were not subject to strong coherent mixing effects near the nozzle.

Further evidence of the influence of coherent structures in flow near to the nozzle can be found in the convection velocity determined from the time delay of maximum two-beam covariance when the sensing beams are separated by a streamwise separation ξ. The variation of convection velocity measured in this way is shown in Fig. 6, and it is clear that in the initial annular mixing region (Fig. 6(a)) the observed convection velocity does not closely follow the local mean velocity profile, whilst in the fully turbulent region (Fig. 6(b)) the observed convection and local mean flow velocity profiles are quite similar. It is clear that in the region close to the nozzle the detection system senses the effectively constant convection velocity of the coherent structures irrespective of the location of the beam intersection as projected into a plane perpendicular to the flow, whilst in the fully turbulent region further away from the nozzle the convection velocity detected is a reflection of the convected motion of the local turbulent structure in the region of the beam intersection point which is quite similar to the local mean velocity.

2.3. *Coherent structure identification by radial/axial cross beam deflection correlations*

More detailed resolution of the actual structure of the large-scale eddies in the flow was obtained by measuring the covariance of the axial beam deflection of one sensing beam (fixed, passing the flow axis, θ_a) with the transverse deflection (θ_{bt}) of the second (traversing) beam. Figure 7 shows the set of cross correlation functions at different radial locations (Y) of the moving beam. These measurements were made using a Nicolet 660B digital signal analysis system to process the photodiode output signals. It can be seen that the correlation functions exhibit a characteristic variation of form that is associated with the particular form of the coherent eddies in the flow and that this variation involves a progressive shift in time delay across the radius combined with variation from an approximately even form of the correlation function with the traversing beam at $Y/d = 0.5$ to an odd function form to either side of this position which reversed in sign on inner and outer edges.

In order to identify the mixing structures which gave rise to the results of Fig. 7, simulated correlations were computed for toroidal vortices crossing the measuring plane of the detecting beams. It was immediately apparent from these computations that

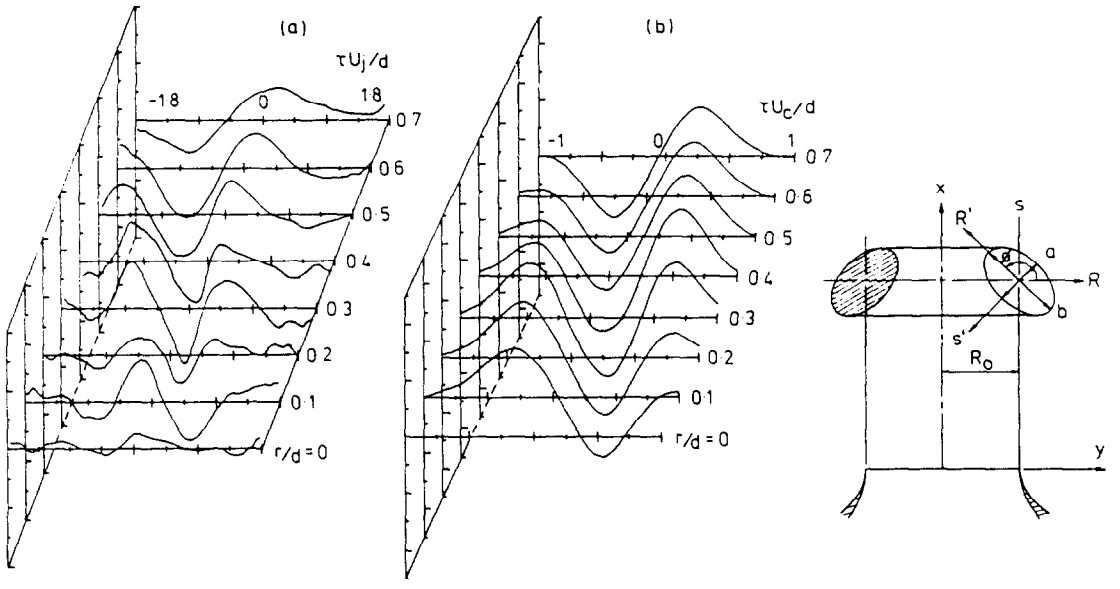

FIG. 7. Distribution of axial–radial beam deflection covariance of cross beams with zero separation. (a) Observed at $x/d = 1.5$. (b) Computed simulation of toroidal ring of elliptical cross-section ($b/a = 3$, $\theta = 5/8\pi$, $r_0/d = 0.5$) (vertical scale: $\overline{\theta_a\theta_{bt}}/(\overline{\theta_a^2}\,\overline{\theta_{bt}^2})^{1/2}$, linear units scale).

the toroidal vortices could not have circular cross-sections if the characteristics of the observed results were to be reproduced. In particular the correlations would not generate progressive movement of the observed correlations along the time delay axis of Fig. 7, and would not give rise to the even form function results observed at the middle of the shear layer. It was found that the only simple form of the density distribution that would give rise to the observed results was a toroidal ring having an elliptical cross-section as illustrated in Fig. 7(b)

$$\rho_a - \rho = \rho_m \exp\left(-4[(R'/b)^2 + (S'/a)^2]\right) \quad (4)$$

where a and b are the minor and major axes of the elliptical cross-section, R' and S' are coordinates measured from the centre of the eddy and ρ_m is the difference in density between air at ambient temperature and at the centre of the toroidal vortex eddy. The computed covariance between the two sensing beams is shown in Fig. 7(b). Whilst it was found the best overall similarity between the results of this elliptical cross-section toroidal model and the experimental observations were obtained with $b/a = 3$, $\phi = 5/8\pi$ and $r_0/d = 0.5$, an exact identification of the optimum of these parameters was not really practicable in view of the rather limited nature of the experimental data which could be obtained. However, it is clear from the results of Fig. 7 that the coherent toroidal structures are of approximately elliptical cross-section with the major axis tilted in the downstream direction on the inside of the toroidal ring as illustrated.

Figure 8 shows an instantaneous spark schlieren photograph of the mixing jet flow together with a simulated reconstruction of the schlieren image of an elliptical cross-section of the type identified in Fig. 7. It is apparent that the cross beam detection system has provided a considerably improved facility to identify the nature of coherent structures in the flow by virtue of the extended time averaging of the two-beam deflection covariance computation by the signal analyser. Whilst it is occasionally possible to detect structures that might resemble the reconstructed image of Fig. 8(b) in actual schlieren photographs, in the main the coherent structures are obscured in such images by the superimposed random disturbances which are present. Figure 8(c) illustrates the geometry of the sheared ring vortex structures which best match the observed correlations as shown in Fig. 7.

2.4. *Transformation of cross beam correlations to spectral energy distributions*

In the fully turbulent region of the mixing flow the cross beam covariance of axial component beam deflections can also form the basis for determining the extent to which the frozen pattern hypothesis [38] applies to the turbulent field and also to determine the energy spectrum of the turbulence by Fourier transformation of the covariance function. Figure 9 shows the comparison of the two-beam density gradient space and time correlations ($R_{\rho'}(\xi)$ and $R_{\rho'}(U_c\tau)$) in the fully turbulent region together with the two point density correlation ($R_\rho(\xi)$ and $R_\rho(U_c\tau)$) where ξ is the axial separation of the two beams, τ the time delay variable as measured by the digital signal analyser and U_c the convection velocity determined from the maxima in covariance of separated two-beam correlations. It can be shown [36] that the correlation

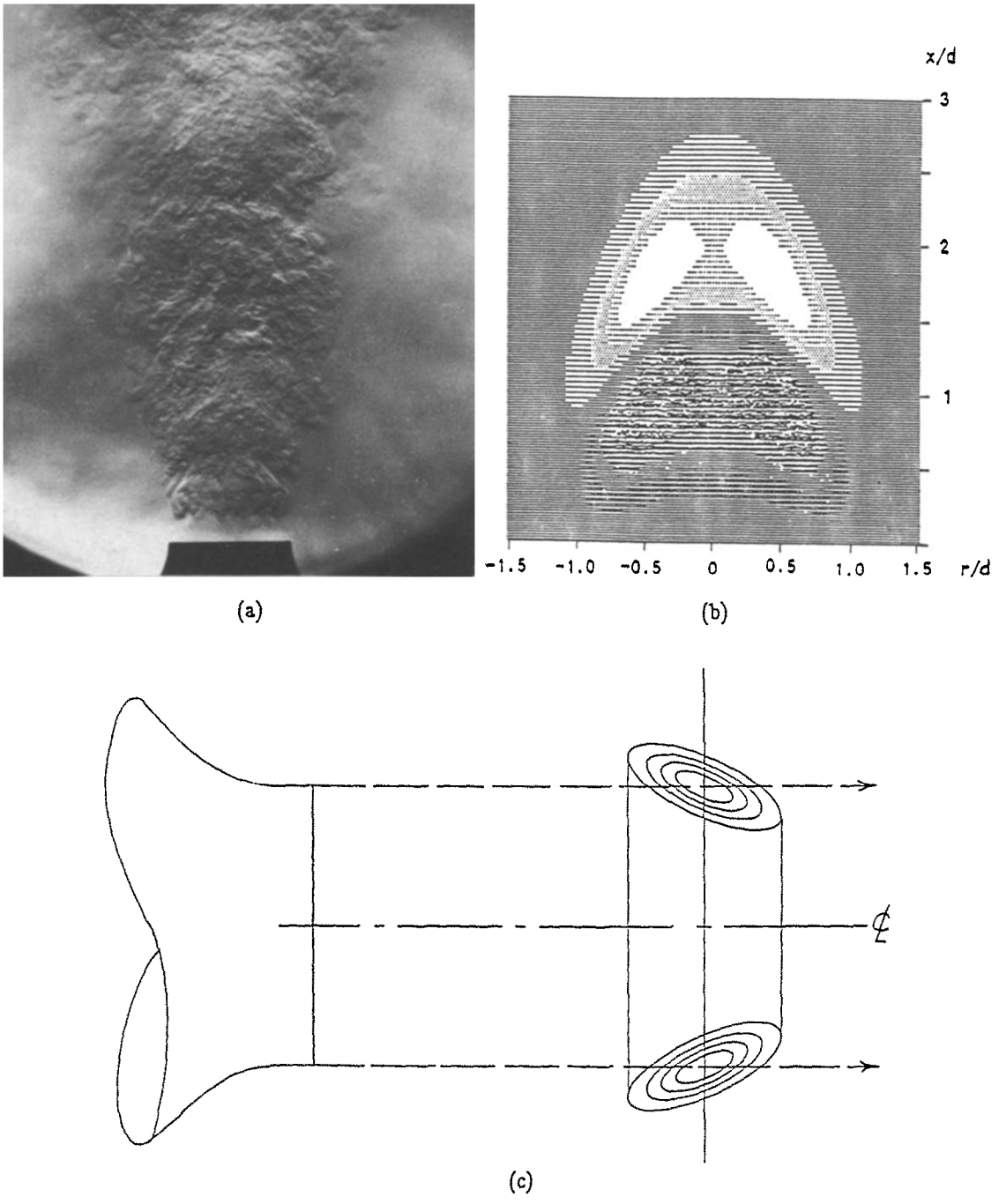

FIG. 8. Instantaneous schlieren visualization records of the mixing flow. (a) Spark photograph of flow from test nozzle. (b) Reconstructed schlieren image of toroidal ring eddy with tilted elliptical cross-section as in Fig. 7. (c) Elliptical cross-section toroidal eddy (contours at 0.2 intervals of maximum density perturbation).

coefficient of density fluctuations can be determined by the relation

$$R_\rho(\xi) = \frac{1}{\xi}\int_0^\xi R_{\rho'}(\xi_1)\,\mathrm{d}\xi_1. \tag{5}$$

It can be seen that the frozen pattern hypothesis is a reasonably good representation of the flow in this case. Following on from this it is possible to determine the spectral distribution of the turbulent fluctuations [36] by transformation first to the schlieren wave number spectrum, $E_S(k_x)$

$$E_S(k_x) = k_x^2/8\pi^3\overline{\rho^2}\int_{-\infty}^{\infty} R_\rho(\xi)\,\mathrm{e}^{-ik_x\xi}\,\mathrm{d}\xi \tag{6}$$

where k_x is the x-direction wave number. We may then

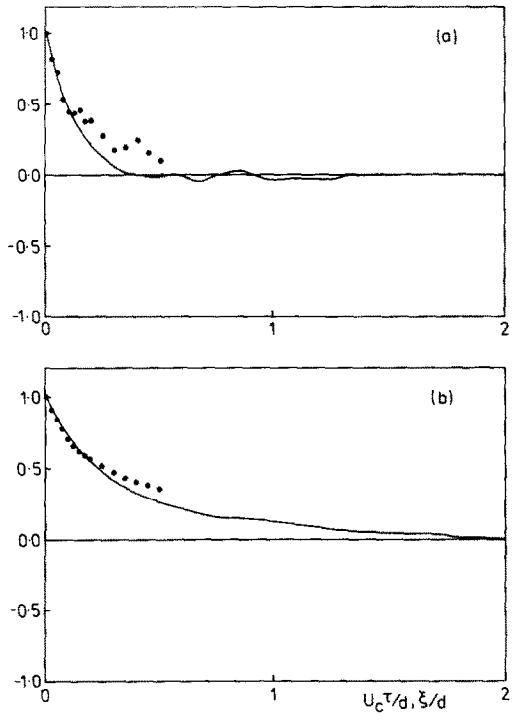

FIG. 9. Cross beam axial deflection cross correlation observations and two point density correlations at $x/d = 15$, $r/d = 0$. (a) Density gradient correlation: points, $R_{\rho'}(\xi/d)$; solid line, $R_{\rho'}(U_c\tau/d)$. (b) Density correlations: points, $R_\rho(\xi)$; solid lines, $R_\rho(U_c\tau)$.

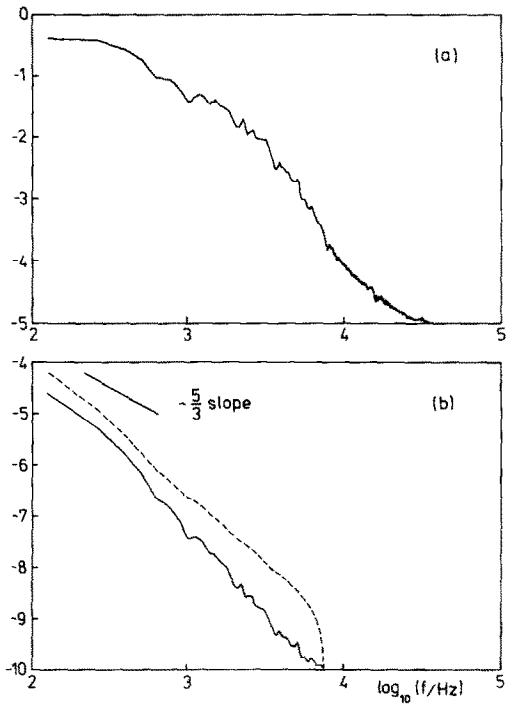

FIG. 10. Spectral distributions at $x/d = 15$, $r/d = 0$. (a) Schlieren energy spectrum ($\log_{10} E_s/2\pi n^2$). (b) Spectra of density fluctuations ($\log_{10} E/2\pi n^2$): dashed line, $E_{3\rho}(k_x, 0, 0)$; solid line, $E_{1\rho}(k_x)$.

proceed to the x component of the three-dimensional wave number spectrum of the density fluctuations

$$E_{3\rho}(k_x, 0, 0) = E_S(k_y)/k_x^2 \tag{7}$$

and thence to the one-dimensional wave number spectrum of the density fluctuations

$$E_{1\rho}(k_x) = \int_{k_x}^{\infty} \frac{E_{3\rho}(k, 0, 0)}{k}\, dk. \tag{8}$$

These spectral distributions are shown in Fig. 10, and it is clear from the results that in the fully turbulent region the turbulent fluctuations in the mixing flow conform fairly well to the expected reduction with wave number for flows where turbulent eddies break up and lead to a distributed and random transfer of energy from large to small scales. The negative slope of the density fluctuation spectra is rather steeper than the form of the Kolmogorov relation in the equilibrium range, but this is to be expected as the overall flow Reynolds numbers in these observations are not extremely large and the dissipation range is not very widely separated from the range of eddy formation. The results indicate clearly that the flow structure has become fully turbulent without significant coherent structural effects at $x/d = 15$. Similar processing of two-beam correlation data at $x/d = 1.5$ also reflected good conformity with the frozen pattern hypothesis, but the correlation functions displayed more periodic behaviour and gave rise to strongly peaked spectral results. These results are not shown here, as the assumptions involved in transformation to the energy spectra [36] are no longer valid when coherent structures are a significant component of the mixing process.

The general conclusions which can be drawn from the optical turbulence observations are that the flow investigated contains strong coherent structures in the initial annular mixing layer ($x/d < 6$ approximately), and that these structures are in the form of toroidal vortices having elliptical cross-sections with the major axis tilted in the downstream direction towards the flow axis. These regular structures move at approximately 0.6 of the jet discharge velocity, but break up in the fully turbulent region ($x/D > 6$). In the fully turbulent region the mixing flow appears more random and shows spectral distributions characteristic of the transfer of mixing energy from the large-scale eddy formation range to the small-scale dissipation range. In the next section the consequences of the coherent structures in the initial region on the thermal diffusion process will be considered.

3. DEVELOPMENT OF MEAN VELOCITY AND TEMPERATURE DISTRIBUTIONS

3.1. *Experimental observation of mean flow velocity and temperature*

The diffusion of the heated jet was observed experimentally at different levels of upstream nozzle exit

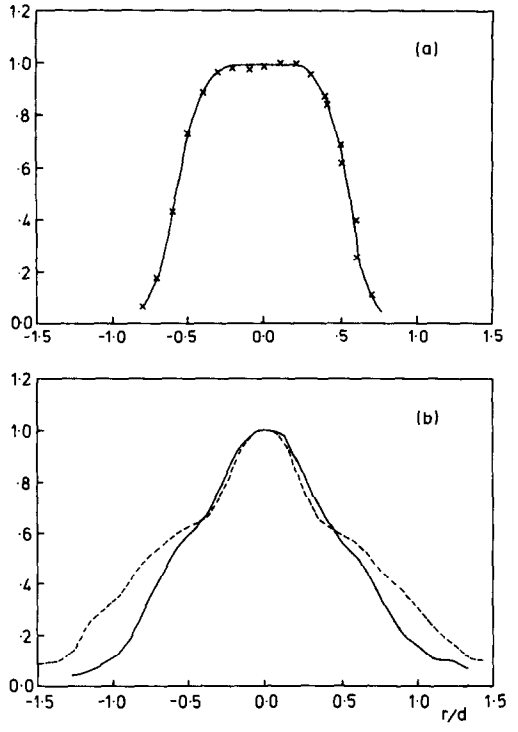

FIG. 11. Influence of excitation level on distribution of observed mean properties across the flow at $x/d = 2$. (a) Mean velocity (U/U_j). (b) Mean temperature $(T-T_0)/(T_j-T_0)$. Nozzle exit plane velocity fluctuation levels: solid line, 3.6%; dashed line, 8.0%.

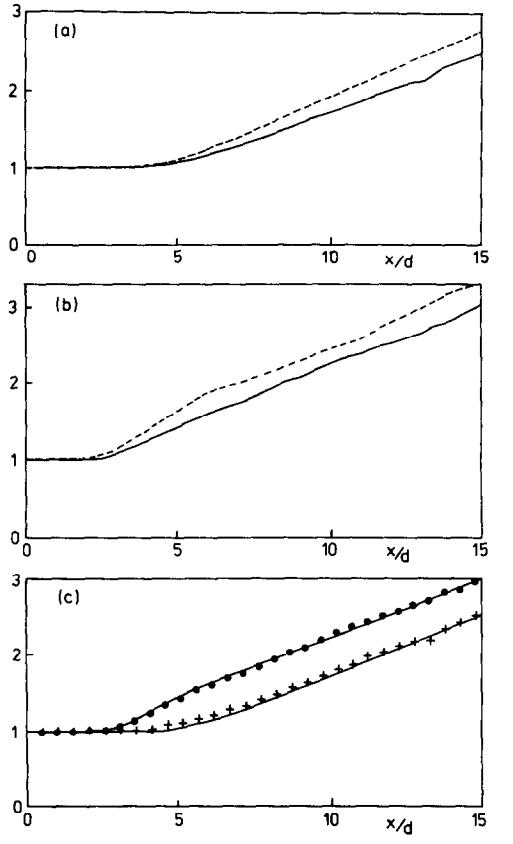

FIG. 12. Distribution of mean properties along centreline. (a) Mean velocity (U_j/U_m). (b) Mean temperature $(T_j-T_0)/(T_m-T_0)$. (c) Comparison of observed (points) and computed (solid lines) results: +, U_j/U_m; ●, $(T_j-T_0)/(T_m-T_0)$ (excitation levels: (a), (b) as for Fig. 11; (c) 8.0% excitation level).

plane excitation by means of pitot tube and electronic manometer, hot wire anemometer, thermocouple probe with temperature compensation circuit and an Analog Devices analogue to digital converter system connected to a data logging computer by a serial link. Probe traverse positions were also passed through this data acquisition system by means of a linear displacement transducer. Mean velocity and mean temperature distributions at two levels of excitation are shown in Figs. 11 and 12. It can be seen that in the initial region at $x/d = 2$ the excitation level has a pronounced effect on the mean temperature profiles which show an increased rate of diffusion at the higher excitation level and the presence of an appreciable inflection in the temperature profile near to $r/d = 0.5$. In contrast the mean velocity profile was not significantly influenced by excitation and showed a smooth decrease of velocity with radius without any local inflection in the observed distributions. These results are in general conformity with the expectation that coherent structures will influence diffusion of passive scalar quantities such as heat, but not the diffusion of momentum [39].

Beyond the initial region of the mixing jet ($x/d > 5$ approximately) the temperature and velocity distributions became more similar and it can be seen (Fig. 13) that both distributions in this region show the influence of the excitation level. The close similarity of these distributions indicates the absence of strong coherent structure effects within this region where the flow mixing is fully turbulent and random in nature. However, it appears from these results that the excitation induced structures produced in the initial region are contributing to the turbulent mixing process in the fully turbulent region by breaking up into random disturbances at the end of the initial region ($x/d \simeq 5$). Thus the coherent structures have an influence which extends beyond the region in which they exist in their original form by fragmenting into turbulent structures which modify the initial condition of the fully turbulent region and thus increase turbulent mixing in that region. This increased turbulent mixing then influences the diffusion of heat and momentum in a similar manner.

3.2. *Coherent flux and k–ε computation of mean flow properties*

To investigate the influence of random and coherent mixing on the diffusion process numerical computation of the heated mixing jet flow was carried out using the discretized conservation equations including turbulent shear and heat transport terms and with additional heat diffusion terms to represent the bulk

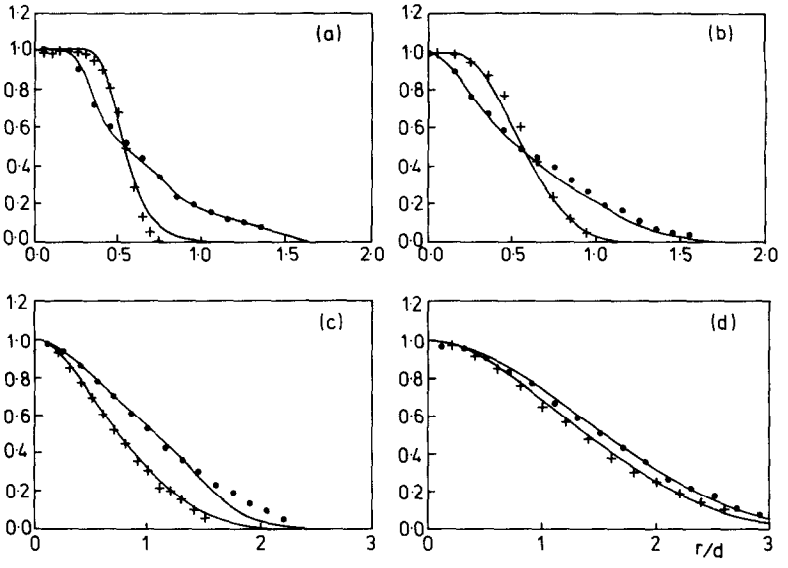

FIG. 13. Observed and computed distributions of mean velocity and temperature (8.0% excitation level). x/D: (a) 1.5; (b) 3.0; (c) 7.5; (d) 15.0 (symbols as Fig. 12(c)).

mixing effects of large-scale structure in the annular mixing region

$$U\frac{\partial U}{\partial x}+V\frac{\partial U}{\partial y}=\frac{\mu}{\rho}\frac{\partial^2 U}{\partial y^2}-\frac{\partial}{\partial y}(\overline{u'v'})$$

and

$$U\frac{\partial T}{\partial x}+V\frac{\partial T}{\partial y}=\frac{k}{\rho c}\frac{\partial^2 T}{\partial y^2}-\frac{\partial}{\partial y}(\overline{v'T'}+\overline{V_p T_p}) \quad (9)$$

where the term $-\overline{V_p T_p}$ denotes the coherent bulk heat transport effect [39]. Coherent mixing is not included in the momentum equation because such terms can reverse in sign instantaneously [40] and average to zero. This behaviour is reflected in the absence of evidence of coherent effects on the mean velocity profile as compared with the mean temperature profile as discussed in the previous section. A standard approach [41] was adopted for the axisymmetric solution of these momentum and energy equations in terms of the stream function or Von Mises plane and elemental control volumes of the type used in the GENMIX programme [42] and its subsequent derivatives. The operation of this programme was first verified by computing the cold mixing jet velocity profile and ensuring that an accurate computational result was obtained by comparison with the reliable experimental data available for the mean velocity distribution [43, 44] in terms of the reduction of centreline velocity with distance from the nozzle (U_m) and the increase of the half velocity width of the flow ($l_{0.5}$). The development of the computational grid following this approach was controlled by the entrainment model [41] at the outer edge of the flow. It was found necessary to relate this entrainment linearly to a distance from the nozzle to ensure a smooth growth of the computational grid through the initial annular and transitional regions of the flow as the original approach [41] which linked the entrainment rate to the velocity profile upstream of the section being computed was found to give rise to very irregular grid development, with very rapid transverse spreading of the grid at $x/D \simeq 25$ as the fully turbulent region was entered. With this modification to achieve uniform grid development the computation gave good agreement with experimental unheated jet data and could be extended from $x/D = 0$ to 60 or beyond if an appropriate model for the dependence of total shear stress on position was introduced. In these initial evaluations of the computational method to establish a regular grid development the turbulent shear stress was modelled in terms of a mixing length which increased linearly with distance from the nozzle to a value of $0.41D$ at $x/D = 6$ and then to $0.82D$ at $x/D = 50$. Subsequent computations of the heated jet mixing were carried out by introduction of k–ε turbulence equations using the values of the coefficients determined previously [45]. For the turbulence energy k

$$\rho U\frac{\partial k}{\partial x}+\rho V\frac{\partial k}{\partial y}=\frac{1}{y}\frac{\partial}{\partial y}\left(y\frac{\mu_t}{\sigma_n}\frac{\partial k}{\partial y}\right)+P-\rho\varepsilon$$

where

$$P=-\rho\left(\overline{uv}\frac{\partial U}{\partial x}+\overline{u^2}\frac{\partial U}{\partial x}+\overline{v^2}\frac{\partial V}{\partial y}+\overline{w^2}\frac{V}{y}\right)$$

$$\mu_t=\rho c_\mu k/\varepsilon$$

and

$$c_\mu=0.09, \quad \sigma_k=1. \quad (10)$$

For the dissipation ε

$$\rho U\frac{\partial \varepsilon}{\partial x}+\rho V\frac{\partial \varepsilon}{\partial y}=\frac{1}{y}\frac{\partial}{\partial y}\left(y\frac{\mu_t}{\sigma_\varepsilon}\frac{\partial \varepsilon}{\partial y}\right)+(C_{\varepsilon 1}P-C_{\varepsilon 2}\rho\varepsilon) \tag{11}$$

where

$$C_{\varepsilon 1}=1.44,\quad C_{\varepsilon 2}=1.92,\quad \sigma_\varepsilon=1.33.$$

The initial development of the jet was found to be quite sensitive to the initial values of k and ε [45] and a trial and error technique with appropriate constants of the turbulence model can be used near the nozzle. In the present work an alternative way of obtaining the starting values of k and ε was employed, by using the mixing length model in the near zone until the mixing layer had spread to the axis. From the initial effective viscosity provided by the mixing length model and an additional parameter, namely the ratio of production to dissipation (R), the initial values of k and ε can be estimated. The equation for turbulence production can be written as

$$P=\mu_t\left(\frac{\partial U}{\partial y}\right)^2-\frac{2}{3}\rho k\left(\frac{\partial U}{\partial x}\right)+2\mu_t\left(\frac{\partial U}{\partial x}\right)^2. \tag{12}$$

Introducing a non-dimensional parameter, the production–dissipation ratio ($R=P/\rho\varepsilon$), we obtain

$$R\rho^2 C_\mu\frac{k^2}{\mu_t}=\mu_t\left(\frac{\partial U}{\partial y}\right)^2-\frac{2}{3}\rho k\left(\frac{\partial U}{\partial x}\right)+2\mu_t\left(\frac{\partial U}{\partial x}\right)^2. \tag{13}$$

In the above equation, apart from k all quantities are known and this quadratic can be solved for k and thus the dissipation determined to start the k–ε based computation.

To start the k–ε model for a flow containing large structures it was assumed that the ratio of turbulent production to dissipation should initially be the same as that for the flows without excitation. With the constants in the mixing length model adjusted to accommodate the higher effective viscosity for prediction of mean velocity profiles in the present experiments, the temperature profile prediction was then achieved by adding the coherent heat flux gradient terms as described.

To determine the nearest position from the nozzle exit for starting the k–ε model computation after using the mixing length model initially, it was found that difficulty in satisfying both the centreline development and the radial profile simultaneously was encountered when starting the k–ε model close to the nozzle. A high ratio of production to dissipation is needed to yield a correct prediction of the centreline decay result. As a consequence, the spreading rate in the near zone was predicted as too large. This may be the reason why a high spreading rate in the self preserving region with a correct half width value has been found previously [45] and that another set of the constants in the turbulence model or the mixing length model must be used. As the starting position of the k–ε model was moved out from the nozzle, the necessary starting ratio decreased. By changing from the mixing length to the k–ε model at $x/d=4.5$ downstream of the nozzle exit (the end of the potential core), the use of the k–ε model as described using a single set of constants in k–ε was then capable of providing a prediction in close agreement with the observed velocity profiles. This is shown in Fig. 11 which compares experimental and computed results determined as outlined above. It can be seen that the assumption of the same production–dissipation ratio for both levels of excitation is verified by this comparison.

In Figs. 12 and 13, the normalized temperature profiles show the significant influence of the coherent radial heat transport. To compute the subsequent development of these profiles, the most suitable model was found to be in the form of a coherent heat flux model, divided into three sections along the axial direction between stations at $x/d=0$, 1.5, 3.0, and 4.5. Within each section, the radial coherent heat transport gradient distribution was represented by the same set of parameters. The peaks in the distribution were always fixed at the same radial position, while the widths were allowed to expand radially according to the shear layer width. The coherent radial heat flux was determined iteratively by matching the computed temperature profiles to those observed as shown in Figs. 12 and 13. Whilst this represents a rather coarse modelling of the bulk mixing effect, the data available was not sufficiently detailed to determine a more accurate axial distribution of bulk mixing effects. The coherent heat flux values shown in Fig. 14 are those required in the computation to match the observed average temperature distributions. To satisfy the conservation of heat for the coherent model used the coherent heat flux is always made to be zero at the last point of the profile computation as seen in Fig. 13. To match the experimental observations the maximum coherent heat flux occurs at $r/d=0.55$, $x/d=1.5$, and a magnitude of approximately 0.035 of the jet flux is needed. The value of the normalized heat flux is comparable to the normalized coherent Reynolds stress in the experiment of Hussain [40], except that the coherent structure Reynolds stress changes sign periodically, and leads to a lower spreading rate of mean velocity profiles as previously discussed. At $x/d=3$, the heat flux was reduced by half in the computation and spreads over a larger radial distance in order to match the observed profiles. A further reduction of coherent heat flux was needed at $x/d=4.5$. The mean temperature profiles obtained by using this model are well predicted as shown in Figs. 12 and 13, having adjusted the required strength and distribution of the coherent heat flux terms as shown in Fig. 14. The total heat flux due to random mixing is also shown in Fig. 14. It can be seen that a broad double peak in the random Reynolds heat flux near the nozzle is a direct result of the shape of the temperature profiles. Far downstream, similar distributions of heat flux and turbulent stress can be

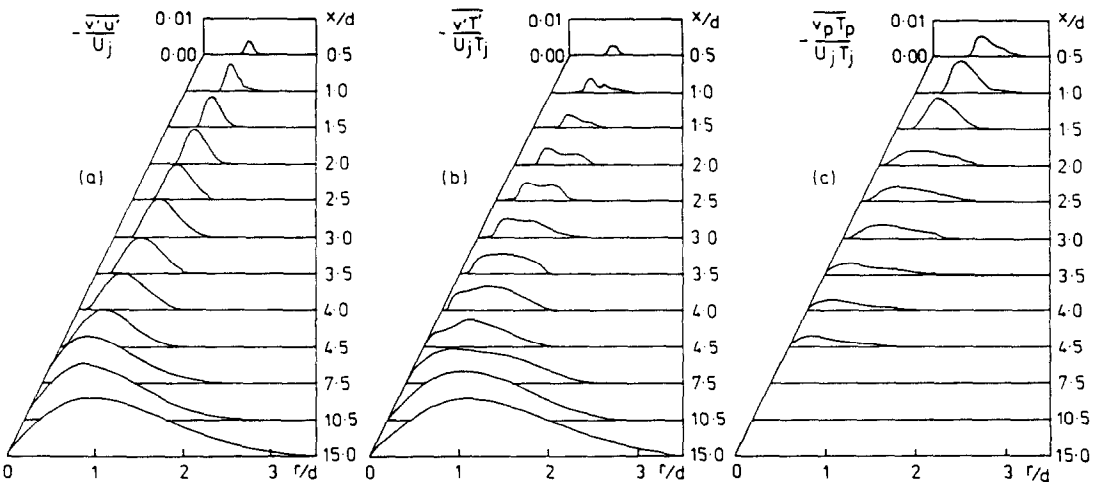

FIG. 14. Distribution of coherent and turbulent mixing parameters required to match observed and computed mean velocity and temperature distributions (Fig. 13). (a) Turbulent shear stress. (b) Turbulent heat flux. (c) Coherent heat flux.

observed. The results demonstrate quite clearly the effect of excitation level on the temperature profile and the peak values of $-u_pT_p/\overline{U_jT_j}$ at $x/d = 2$, $r/d = 0.5$ decreases systematically from 0.043 at 8% excitation, to 0.033 at 3.6% excitation and to approximately 0.025 at 1.3% excitation.

The parameters in the elliptical torus coherent structure density model provide a basis for magnitude comparison with the coherent heat flux. Two unknown parameters, the streamwise space interval of the vortices or time average period of passing of the structures and the magnitude of density fluctuations at their centre, can be determined by matching the autocorrelation of the single beam axial deflections and the coherent heat flux from the computation provided in this section. Two sets of data are needed because two unknowns are to be determined. The reason for the use of the autocorrelation or single beam angular fluctuation intensity instead of the cross correlation in this magnitude estimation is that any variation of the parameters of the observed density structures, such as phase shifts between detection beams, will not influence the signal of the single beam significantly. We also assume that the random mixing components do not contribute strongly to the observed autocorrelation, although the relatively smaller random mixing in the annular region will somewhat reduce the coherence coefficients which are obtained experimentally. It should be noted that the averaging of fluctuations in the vortex model is carried out by subtracting the mean component out to obtain consistency in comparison with the experimental data. From the density model in equation (4) we can write the single beam intensity of fluctuation due to the passage of vortices spaced by a distance L in the streamwise direction as

$$\overline{\theta_\eta^2} = \frac{1}{L}\int_{-L/2}^{L/2} A_{gd}^2 \rho_m^2 \left[\int_{-\infty}^{\infty} \frac{\partial e^{-A}}{\partial x}\,dy\right]^2 dt \quad (14)$$

where $A = 4\{(R'/b)^2 + (S'/a)^2\}^{1/2}$ and A_{gd} is the Gladstone–Dale constant relating refractivity and density variations [35]. If we assume for the moment that the turbulent heat flux can be neglected by comparison with the coherent heat flux in the initial region, then an estimate of the magnitude of the time derivative of temperature is given by

$$\left[\frac{\partial T}{\partial t}\right] \sim \frac{1}{r}\frac{\partial(-r\overline{v_pT_p})}{\partial r}. \quad (15)$$

Integration then yields, if $[\partial T/\partial t] \sim U_c(\partial T/\partial x)$, an estimate of the average coherent heat flux as

$$-\overline{v_pT_p} \sim \frac{1}{r}\int_0^r rU_c\frac{\partial T}{\partial x}\,dr + C. \quad (16)$$

Substituting the density gradient from the model (equation (4)) for the temperature gradient we have an estimate of the coherent heat flux due to the regular vortices as

$$-\overline{v_pT_p} \sim \frac{1}{L}\int_{-L/2}^{L/2} A_{gd}\rho_m \frac{1}{r}\left[\int_0^r rU_c\frac{P}{R\rho^2}\frac{\partial e^{-A}}{\partial x}\,dr\right]dx \quad (17)$$

where $A = 4[(R'/b)^2 + (S'/a)^2]^{1/2}$, L is the average ring vortex streamwise spacing, P the pressure and a, b the minor and major axes of the elliptical vortex (e^{-4} position).

Figure 15 shows the relation between ρ_m and L obtained by matching the values of the coherent heat flux which was required in the numerical computation of the mean temperature field and the angular fluctu-

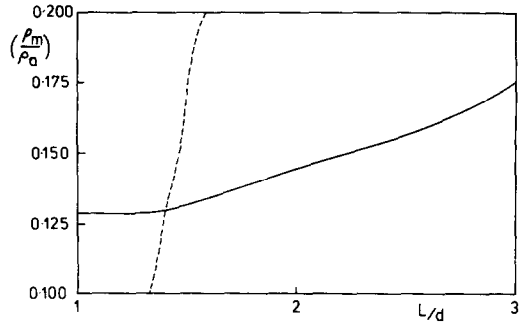

FIG. 15. Variation of amplitude of coherent structure density excursion and spacing of structures modelled by equation (4). Solid line, to match observed beam fluctuations $\overline{\theta^2}(Y)$. Dashed line, to match required coherent heat flux.

ating deflection data ($\overline{\theta_\eta^2}(Y)$) in equation (17). Simultaneous matching occurs at $\rho_m = 0.13$ and $L/d = 1.4$. Sheared vortex ring spacings of 1.4 times the jet diameter were thus generally consistent with the computed coherent radial heat flux and also with estimations of vortex spacings slightly less than the jet nozzle diameter at $x/d = 1.5$ obtained from the frequency of peaks in the schlieren signals and spectra close to the nozzle. Schlieren spectra at $x/d = 1.5$ showed a sharp peak at $St = fd/U_j = 0.64$ whilst separated beam cross correlations indicated a convection velocity $U_c/U_j = 0.7$, these figures thus suggesting a spacing between vortices of 0.92 of the nozzle diameter. It should be noted that in the process of finding the average spacing and amplitude of density fluctuations, matching of the autocorrelation or variance of angular deflections cannot be an exact process since the random turbulent components are not represented in the approximation of equation (17). Thus it appears that a somewhat high value of the average vortex spacing has been obtained by matching the coherent heat flux with the frequency of regular structures in the shear layer in this way. However, it is clear that there is a good overall degree of consistency between the coherent heat flux required to produce the necessary thermal diffusion in the numerical computation, and the spacing to match the observed thermal diffusion of the observed coherent structures in the flow near the nozzle. The strength of the maximum density variation at the core of the vortices ($\rho_m/\rho_j = 0.13/1.06 = 0.12$) obtained by matching in equation (17) is also quite consistent with the formation of these vortices by bulk entrainment across the mixing layer between the jet and the surroundings ($(\rho_o - \rho_j)/\rho_j = 0.14$).

4. CONCLUSIONS

Operation of the heated nozzle flow with differing levels of acoustic disturbance and associated velocity fluctuations across the otherwise smooth exit flow has demonstrated the influence of upstream excitation on the thermal mixing process. The mean flow field velocity and temperature distributions show clearly that the coherent structures induced in the mixing layer do not significantly modify the mean velocity in the annular mixing layer but they do substantially contribute to the passive scalar transport across the flow and thereby influence the mean temperature profiles. In the fully turbulent region of the mixing flow the coherent structures break up and similarity of velocity and temperature profiles is gradually re-established. However, the residual effects of the coherent structure are evident in this region by an appreciable increase in the decay of both mean velocity and temperature at the centreline due to excitation.

Optical observations of the thermal mixing process have given clear evidence of the presence of coherent structures in the initial annular mixing region through the characteristics of cross beam correlations. The results indicate that the coherent structures are in the form of toroidal ring vortices which have an elliptical cross-section in the torus, the major axis being inclined in the downstream direction and towards the centreline of the flow. Further away from the nozzle in the fully turbulent mixing region the optical observations show that the temperature field has reverted to a more random mixing process with the expected form of spectral and correlation functions.

Computations of the flow field using a k–ε model indicate that the radial coherent heat flux is substantial in the initial annular mixing layer and exceeds the turbulent transport in that region. The magnitude of this coherent heat flux is consistent with mixing of vortices moving with the flow with a streamwise spacing comparable to the nozzle diameter. This spacing is consistent with the frequency of strongest mixing fluctuations observed optically near to the nozzle on the basis that the disturbances propagate at 0.7 of the jet velocity. Thus, it can be said that the optical evidence of the coherent structures is consistent with their effect on the mean temperature distributions in terms of the radial coherent heat transport. The maximum coherent radial heat flux decreased steadily from 0.043 of the jet heat flux when the coherent mixing was induced by an 8% level of excitation velocity fluctuations at the jet exit to 0.025 of the jet heat flux at an excitation level of 1.3%.

REFERENCES

1. P. Paranthoen, A. Fouari, A. Dupont and J. C. Lecordier, Dispersion measurements in turbulent flows (boundary layer and plane jet), *Int. J. Heat Mass Transfer* **31**, 153–165 (1988).
2. F. C. Lockwood and H. A. Moneib, Fluctuating temperature measurements in a heated round free jet, *Combust. Sci. Technol.* **22**, 63–81 (1980).
3. R. A. Antonia, On a heat transport model for a turbulent plane jet, *Int. J. Heat Mass Transfer* **28**, 1805–1812 (1985).
4. A. J. Chambers, R. A. Antonia and L. Fulachier, Turbulent Prandtl number and spectral characteristics of a turbulent mixing layer. *Int. J. Heat Mass Transfer* **28**, 1461–1468 (1985).

5. L. Fulachier and R. A. Antonia, Spectral analogy between temperature and velocity fluctuations in several turbulent flows, *Int. J. Heat Mass Transfer* **27,** 987–997 (1984).
6. J. Y. Zhu, R. M. C. So and M. V. Otugen, Turbulent mass flux measurements using a laser/hot wire technique, *Int. J. Heat Mass Transfer* **31,** 819–829 (1988).
7. R. A. Antonia, A. J. Chambers and L. W. B. Browne, Relations between structure functions of velocity and temperature in a turbulent jet, *Exp. Fluids* **1,** 213–219 (1983).
8. R. A. Antonia and L. W. B. Browne, The destruction of temperature fluctuations in a turbulent plane jet, *J. Fluid Mech.* **134,** 67–83 (1983).
9. R. Chevray and N. K. Tutu, Intermittency and preferential transport of heat in a round jet, *J. Fluid Mech.* **88,** 133–160 (1978).
10. S. Tavoularis and S. Corrisin, Effects of shear on the turbulent diffusivity tensor, *Int. J. Heat Mass Transfer* **28,** 265–276 (1985).
11. A. Toompu, A phenomenological model for the passive scalar variance transformation in a turbulent fluid, *Int. J. Heat Mass Transfer* **28,** 1773–1781 (1985).
12. J. Simonek, A model of eddy viscosity and eddy diffusivity of heat, *Int. J. Heat Mass Transfer* **26,** 479–508 (1983).
13. S. V. Patankar, Some recent developments in heat transfer, *ASME J. Heat Transfer* **110,** 1037–1045 (1988).
14. B. E. Launder, On the computation of convective heat transfer in complex turbulent flows, *ASME J. Heat Transfer* **110,** 1112–1128 (1988).
15. R. H. Pletcher, Progress in turbulent forced convection, *ASME J. Heat Transfer* **110,** 1129–1144 (1988).
16. J. F. Sini and I. Dekeyser, Numerical prediction of turbulent plane jets and forced plumes by use of the k–ε model of turbulence, *Int. J. Heat Mass Transfer* **30,** 1787–1801 (1987).
17. M. Sokolov, A. K. M. F. Hussain, S. J. Kleis and Z. D. Husain, A turbulent spot in an axisymmetric free shear layer. Part I: *J. Fluid Mech.* **98**(1), 65–95 (1980), Part II: *J. Fluid Mech.* **98,** 97–135 (1980).
18. H. E. Fiedler and P. Mensing, The plane turbulent shear layer with periodic excitation, *J. Fluid Mech.* **150,** 281–309 (1985).
19. A. K. M. F. Hussain and M. A. Z. Husan, Turbulence suppression in free turbulent shear flows under controlled excitation, *J. Fluid Mech.* **150,** 159–168 (1985).
20. J. Lepicovsky, K. K. Ahuja and R. H. Burrin, Tone excited jets, Part III: flow measurements, *J. Sound Vibr.* **102**(1), 71–91 (1985).
21. M. R. Davis, Coherence between large scale jet mixing structure and its pressure field, *J. Fluid Mech.* **116,** 31–57 (1982).
22. M. R. Davis, Phase spectral evidence for vortex structures in turbulent mixing, *J. Sound Vibr.* **116,** 303–321 (1987).
23. J. Jimenez, M. Cogollos and L. P. Bernal, A perspective view of the plane mixing layer, *J. Fluid Mech.* **152,** 125–143 (1985).
24. G. M. Corcos, S. J. Lin and F. S. Sherman, The mixing layer: deterministic models of a turbulent flow. Part I: *J. Fluid Mech.* **139,** 29–65 (1984). Part II: *J. Fluid Mech.* **139,** 67–95 (1984).
25. A. K. M. F. Hussain and K. B. M. Q. Zaman, An experimental study of organized motions in the turbulent plane mixing layer, *J. Fluid Mech.* **159,** 85–104 (1985).
26. M. Ikeda, Finite disturbances and growing varieties in a two dimensional jet, *J. Fluid Mech.* **80**(3), 401–421 (1977).
27. K. B. M. Q. Zaman and A. K. M. F. Hussain, Natural large scale structures in the axisymmetric mixing layer, *J. Fluid Mech.* **138,** 325–351 (1984).
28. S. Kamori and H. Ueda, The large scale coherent structure in the intermittent region of the self preserving round free jet, *J. Fluid Mech.* **152,** 337–359 (1985).
29. F. K. Browand and J. R. Troutt, The turbulent mixing layer: geometry of large vortices, *J. Fluid Mech.* **158,** 489–509 (1985).
30. S. E. Widnall, D. B. Bliss and C. Y. Tsai, The stability of short waves on a vortex ring, *J. Fluid Mech.* **66,** 35–47 (1974).
31. W. C. Reynolds, Computation of turbulent flows, *Ann. Rev. Fluid Mech.* 83–208 (1976).
32. S. Byggstoyl and W. Kollman, Closure model for intermittent turbulent flows, *Int. J. Heat Mass Transfer* **24,** 1811–1822 (1982).
33. C. G. Speziale, Galilean invariance of subgrid scale stress models in the large eddy simulation of turbulence, *J. Fluid Mech.* **156,** 55–62 (1985).
34. P. G. Mason and N. S. Callen, On the magnitude of the subgrid scale eddy coefficient in the large eddy simulation of turbulent channel flow, *J. Fluid Mech.* **162,** 439–462 (1986).
35. M. R. Davis, Intensity, scale and convection of turbulent density fluctuations, *J. Fluid Mech.* **70,** 463–479 (1975).
36. H. Winarto and M. R. Davis, Fluctuations of density pressure and temperature in a turbulent mixing region, *Proc. R. Soc. London* **A395,** 203–228 (1984).
37. G. N. Minerbo and M. E. Levy, Inversion of Abel's integral equations by means of orthogonal polynomials, *SIAM J. Numer. Analysis* **6,** 598–616 (1969).
38. A. A. Townsend, *The Structure of Turbulent Shear Flow*. Cambridge University Press, Cambridge (1976).
39. J. O. Hinze, *Turbulence*. McGraw-Hill, New York (1975).
40. A. K. M. F. Hussain, Coherent structures of perturbed and unperturbed jets. In *Lecture Notes in Physics*, Vol. 136. Springer, Berlin (1981).
41. D. B. Spalding, *Genmix—A General Computer Programme for Two Dimensional Parabolic Phenomena*. Pergamon Press, Oxford (1977).
42. S. V. Patankar, *Numerical Heat Transfer and Fluid Flow*. Hemisphere, Washington, DC (1980).
43. I. Wygnanski and H. Fiedler, Some measurements in the self preserving jet, *J. Fluid Mech.* **38,** 557–612 (1969).
44. P. O. A. L. Davies, M. J. Fisher and M. J. Barratt, The characteristics of the turbulence in the mixing region of a round jet, *J. Fluid Mech.* **15,** 337–367 (1963).
45. W. Rodi, *Turbulent Buoyant Jets and Plumes*. Pergamon Press, Oxford (1962).

INFLUENCE DES GRANDS TOURBILLONS SUR LE MELANGE THERMIQUE

Résumé—L'influence du niveau d'excitation en amont sur le mélange de la chaleur et de la quantité de mouvement dans un jet circulaire est étudiée et on trouve qu'il y a une dépendance directe entre le transport cohérent de chaleur et l'intensité de cette excitation. Les structures cohérentes n'influencent pas les distributions de vitesse moyenne près de la tuyère, mais plus en aval elle se brisent et elles contribuent à un accroissement semblable du mélange de chaleur et de quantité de mouvement dans l'écoulement. Des observations optiques montrent que les structures cohérentes sont en forme de tourbillons toriques ayant approximativement une section droite elliptique dans le tore et qu'elles se déplacent à une vitesse qui est en rapport avec l'intensité du flux thermique cohérent dans la région annulaire initiale de l'écoulement.

EINFLUSS GROSSRÄUMIGER WIRBEL AUF THERMISCHE MISCHVORGÄNGE

Zusammenfassung—Mischungsvorgänge (im Hinblick auf Wärme und Impuls) in einem kreisrunden Strahl werden abhängig von der Intensität einer stromauf eingebrachten Anregung untersucht. Es zeigt sich eine direkte Abhängigkeit zwischen der Stärke dieser Anregung und dem dadurch verursachten Wärmetransport. Die sich ergebenden Strukturen haben keinen Einfluß auf die Verteilung der mittleren Geschwindigkeit nahe der Düse, sie brechen jedoch an stromabwärts gelegenen Stellen hervor und tragen dann zu einer verstärkten Vermischung in der Strömung bei. Visuelle Beobachtungen zeigen, daß die vorhandenen Strukturen die Gestalt von torusförmigen Wirbeln aufweisen, wobei der Torus näherungsweise elliptischen Querschnitt hat.

ВЛИЯНИЕ БОЛЬШИХ ВИХРЕЙ НА СМЕШЕНИЕ ТЕПЛОТЫ

Аннотация—Исследуется влияние уровня возбужденного состояния вверх по течению на смешение теплоты и количества движения в круглой струе, и обнаружена прямая зависимость когерентного теплопереноса от силы возбуждения. Когерентные структуры не влияют на распределение средних скоростей вблизи сопла, но разрушаются дальше вниз по течению и затем способствуют усилению аналогичного смешения средних значений теплоты и количества движения в потоке. Оптические наблюдения показывают, что когерентные структуры имеют форму тороидальных вихрей с почти эллиптическими поперечными сечениями тора и наблюдаются при скорости, соответствующей величине когерентного теплового потока в начальной кольцевой области течения.